Optical-depth scaling of light scattering from a dense and cold atomic ^{87}Rb gas

K. J. Kemp, S. J. Roof, M. D. Havey, I. M. Sokolov, D. V. Kupriyanov, and W. Guerin

Phys. Rev. A **101**, 033832 — Published 20 March 2020

DOI: 10.1103/PhysRevA.101.033832

Optical-depth scaling of light scattering from a dense and cold atomic ^{87}Rb gas

K.J. Kemp, S.J. Roof, and M.D. Havey

Old Dominion University, Department of Physics, Norfolk, Virginia 23529

I.M. Sokolov

Department of Theoretical Physics, Peter the Great St.-Petersburg Polytechnic University, 195251, St.-Petersburg, Russia and Institute for Analytical Instrumentation, Russian Academy of Sciences, 198103, St.-Petersburg, Russia

D.V. Kupriyanov

Center for Advanced Studies, Peter the Great St.-Petersburg Polytechnic University, 195251, St.-Petersburg, Russia and Quantum Technologies Center, M.V. Lomonosov Moscow State University, Leninskiye Gory 1-35, 119991, Moscow, Russia

W. Guerin

Université Côte d'Azur, CNRS, Institut de Physique de Nice, France

(Dated: February 24, 2020)

We report investigation of near-resonance light scattering from a cold and dense atomic gas of ^{87}Rb atoms. Measurements are made for probe frequencies tuned near the $F = 2 \rightarrow F' = 3$ nearly closed hyperfine transition, with particular attention paid to the dependence of the scattered light intensity on detuning from resonance, the number of atoms in the sample, and atomic sample size. We find that, over a wide range of experimental variables, the optical depth of the atomic sample serves as an effective single scaling parameter which describes well all the experimental data.

I. INTRODUCTION

Study of light interacting with cold and ultracold atomic gases is an active area of experimental and theoretical research [1, 2]. The subject appears to be deceptively simple, corresponding in many cases to a single weak probe beam scattering from a small cloud of cold atoms. However, under most realistic situations, the atoms in such a sample interact not only with the incident radiation field, but also with the light scattered by all the other atoms in the sample. The ensembles may then be viewed as many-body physical systems, and can display emergent complexity. The optical response reveals a collective optical response that differs significantly from that of a dilute, optically thin atomic ensemble.

Over the past few years, there have been a large number of reports on collective or cooperative effects in light scattering by atoms. For instance, steady-state experiments have revealed collective effects, such as lensing [3], light diffusion [4, 5], changes in the radiation pressure force [6–8], etc. Because of potentially important consequences for clock technology [9], the question of collective shifts of the resonance line, in particular, raised a lot of discussions [10–15] and experiments [16–24]. Even without any shift, changes in the line shape, collective broadening and saturation of the amount of scattered light have been observed in several experiments with different parameters and geometries, and interpreted somewhat differently [4, 21, 23–27].

In many of these studies, collective changes in the atomic response are measured and displayed as a function of the atomic density. The results are then attributed to dipole-dipole interactions and presented in the context of the

coupled dipole model. This approach basically includes all the essential physics (attenuation, diffraction, refraction, multiple scattering, collective frequency shifts, etc). In a typical cold-atom experiment, however, the atomic density cannot be readily changed independently of other parameters such as the sample size or the atom number. Then it may be difficult to find if the measured collective effect really depends on the density, on the optical thickness, the number of atoms, or on something else all together. Then, even though excellent results are often obtained from the coupled-dipole model, other approaches such as the Beer-Lambert Law or random walk simulations are valuable and can allow identification of which physical ingredients are really necessary to explain the data.

In this paper, we report measurements of the scattered light intensity from a cloud of cold ^{87}Rb atoms. By changing the number of atoms and the size of the sample, we have varied the optical depth through the center of the trap by about a factor of 10^3. This range is large enough to encompass an optically thin sample on one hand, and emergence of the so-called shadow effect on the other. All measurements are found to be in good agreement with microscopic and fully quantum calculations of the light scattering processes. We find also that over the full and wide range of optical depths the experimental data are well described by a random walk simulation of light transport in the atomic medium; in this model the optical depth serves as an effective single scaling parameter which quantitatively agrees with all the data. A Beer-Lambert's law argument similarly shows a single parameter scaling with the optical depth.

In the following sections we first describe the experimental arrangement and measurement scheme. This is followed by presentation of the experimental results and comparison with quantum microscopic calculations. We follow this by a description of our random walk simulations, Beer-Lambert Law scaling, and comparison of the simulations with the peak optical depth dependence of the experimental data.

II. EXPERIMENTAL ARRANGEMENT

The basic experimental scheme has been described in detail elsewhere [28]; here we provide only an outline of details necessary to understand the experimental approach and results. In the basic approach, we follow a multistep process to produce cold atom samples confined by a far off resonance trap (FORT). Initially, ^{87}Rb atoms are loaded into a 3-dimensional magneto-optical trap (MOT), with a density distribution that can be approximated as Gaussian. The MOT is characterized using methods similar to those in [28]. The physical size and temperature of the MOT are found by directly measuring the radius of a fluorescence image projected onto a CCD camera (pixel resolution of 24 μm x 24 μm). The number of atoms trapped in the MOT is measured through traditional absorption imaging. The number is independently measured by using an optical pumping approach, as described in [29]. We find that normally we have about 450 million atoms contained in the MOT. At this stage of sample preparation, the distribution of atoms among the $F = 2$ Zeeman states is not known. Most groups assume however that the atoms plausibly have the atoms equally distributed among the Zeeman states; we assume that here. This hypothesis leads to an effective light scattering cross-section of $7/15(3\lambda^2/2\pi)$.

A small fraction of the MOT atoms is then loaded into a Far-Off-Resonance Trap (FORT). This trap consists of a single laser beam ($\lambda = 1064$ nm) focused to a beam waist ω_* of about 20 μm. This quantity was measured in an auxiliary experiment using a scanning knife edge to determine the beam shape and size around the focus. The longitudinal scale is given by the Rayleigh range, defined as $z_r = \pi\omega_*^2/\lambda$, which is about 900 μm in our case. The intensity gradient of the focused light, along with being far detuned from resonance, creates a potential well in the

ground state in which the atoms can be trapped. During the loading process, the MOT trapping laser is detuned $\sim 10\gamma$ below resonance and the repumping laser is attenuated by $\sim 99\%$. This reduces the radiation pressure and creates a compressed MOT, which has a better spatial overlap with the FORT laser beam. Atoms excited with the MOT trapping laser tuned near the $F = 2 \rightarrow F' = 2$ transition undergo inelastic Raman transitions, resulting in loading into the lower $F = 1$ ground level. After a loading time of 70 ms, the trapping and repumping lasers are fully extinguished, along with the external magnetic field. Starting with an initial load of $1.3(2) \times 10^6$ atoms, the FORT laser is kept on for a minimum of 200 ms, until the sample is approximately thermalized with $7.8(1) \times 10^5$ atoms at a temperature on the order of 100(5) μK. The FORT atomic density distribution ρ is approximated by a Gaussian distribution as $\rho = \rho_0 \exp(-\frac{r^2}{2r_0^2} - \frac{y^2}{2y_0^2})$ with a radial size r_0, longitudinal radius y_0, and peak density ρ_0. This frequently-made estimate is based on the observation that the atom distribution is dominantly located spatially at small y, such that y is smaller than the Rayleigh length for the trap.

The peak density is determined from the definition $\rho_0 = N/(2\pi)^{3/2} r_0^2 y_0$ and measurements of N, r_0, and y_0 and the temperature T. We described in an earlier paragraph measurement of N by two methods. The longitudinal size $y_0 = 259$ μm is sufficiently large to be measured directly by fluorescence imaging using the CCD, which has a pixel resolution of 24 μm x 24 μm.) The transverse size of $r_0 = 3.0$ μm is too small to be directly measured that way. Instead, we make measurements of the highest transverse parametric resonance frequency (as driven by weak amplitude modulation of the trap depth), which appears at twice the harmonic oscillator frequency ω. Measurement of the FORT temperature, and the transverse confinement allow determination of $r_0^2 = k_B T/m\omega^2$.

Once the atomic sample is thermalized, the FORT trapping laser is turned off. Initially the atoms are repumped into the $F = 2$ ground state to prepare for probing on the $F = 2 \rightarrow F' = 3$ transition. After an optical pumping phase of about 8 μs, nearly all of the atoms are transferred to the $F = 2$ level. After another 2 μs, a near-resonance low intensity (0.1 I_{sat}) probe laser is flashed for 1 μs. As shown in Fig.1(b) the probe beam is linearly polarized, creating by optical excitation an axially symmetric atomic polarization (alignment) in the excited $F = 3$ level with reference to the probe electric field symmetry axis. This in turn modifies the emission diagram, generating an anisotropic diagram of spatial fluorescence. This is a rather small effect, even for an optically thin atomic sample, and results in an intensity difference of 12 %, relative to the isotropic case, on the equatorial plane, and 24 % at the poles. For the fluorescence geometry of our experiment, this is a 7.9 % effect for single scattering from the atomic cloud. For the case of multiple scattering, these are even smaller effects at least for ^{85}Rb, as reported earlier [30]. These two effects are steady state and are hidden in the global rescaling of the data. We thus ignore these small effects in further discussion of the data.

The probe is offset from resonance by a detuning $\Delta = f - f_0$, where f_0 is the bare atomic resonance frequency. As shown schematically in Fig. 1, the probe beam is spatially much larger than the atomic sample, with a e^{-2} radius of 4.5 mm, and as shown in Fig. 1(b) is incident upon the sample at an oblique angle. Fluorescence detection of the fluorescence is also made at an oblique angle (viewing down the x-axis). Following an initial measurement, the sample is allowed to continue to expand and is probed again 40 μs after the initial flash. This process continues for a total of 10 probe pulses up to a total expansion time of 370 μs. The sample expands from an initial volume with radii $r_0 = 3.0$ μm and $y_0 = 259$ μm to final radii of $r_0 = 33.4$ μm and $y_0 = 261$ μm. The fluorescence from the sample is collected without regard to light polarization for all 10 pulses and focused into a multimode fiber connected to an infrared sensitive photomultiplier tube (PMT). The output of the PMT is directed without preamplification

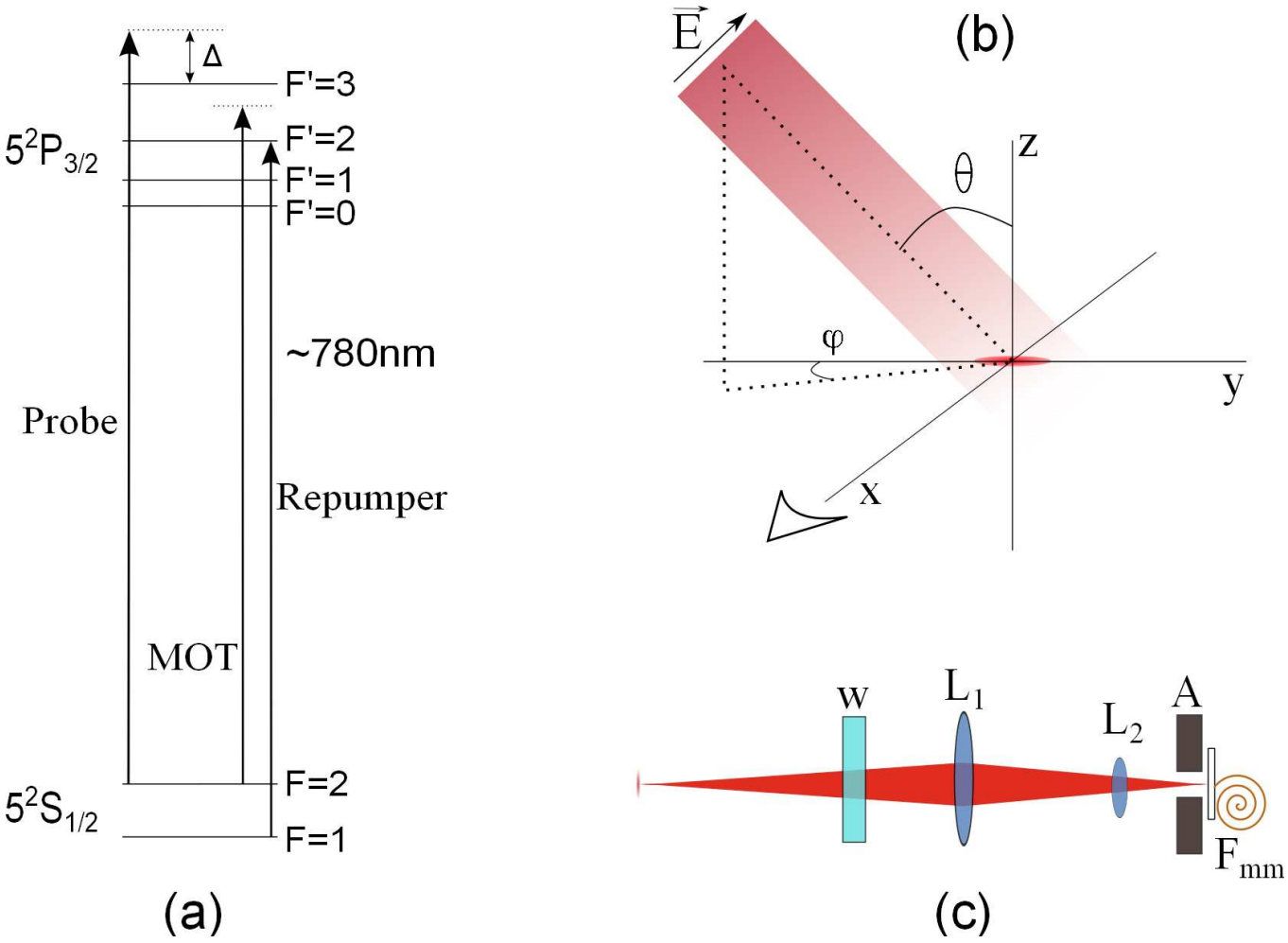

FIG. 1: The basic experimental scheme. (a) Relevant ^{87} *Rb* energy levels. (b) Geometry of probe optical excitation and fluorescence collection. The angles $\theta = 23$ degrees, and $\phi = 30$ degrees. (c) Fluorescence detection arm, viewing down the x-axis. Light is detected in the far field through a window (w) and focused into a 600 μm diameter multimode optical fiber F_{mm} with a pair of lenses L_1 and L_2 as shown.

to a multichannel scaler having 40 ns time resolution. For the results presented in this paper, this time signal was integrated over the duration of each individual pulse to show the total amount of fluorescence for each sample size, all while maintaining the same number of atoms.

In order to sample a broader range of atomic sizes and densities, the number of atoms can also be changed. The peak density of the sample depends on the holding time of the FORT; background gas collisions decrease the number of atoms within the sample. At the longest hold time used for these measurements (2.5 s), the number of atoms is reduced to $1.8(7) \times 10^5$. In Fig 2, the peak density for each sample holding time as a function of expansion time is shown. Finally, we also studied the dependence of the scattered light intensity on probe detuning at the highest possible density for our thermalized sample. Using an acousto-optical modulator (AOM) in a double-pass setup, the frequency of the probe laser was tuned over a range of nearly 60 MHz while maintaining a constant probe optical power.

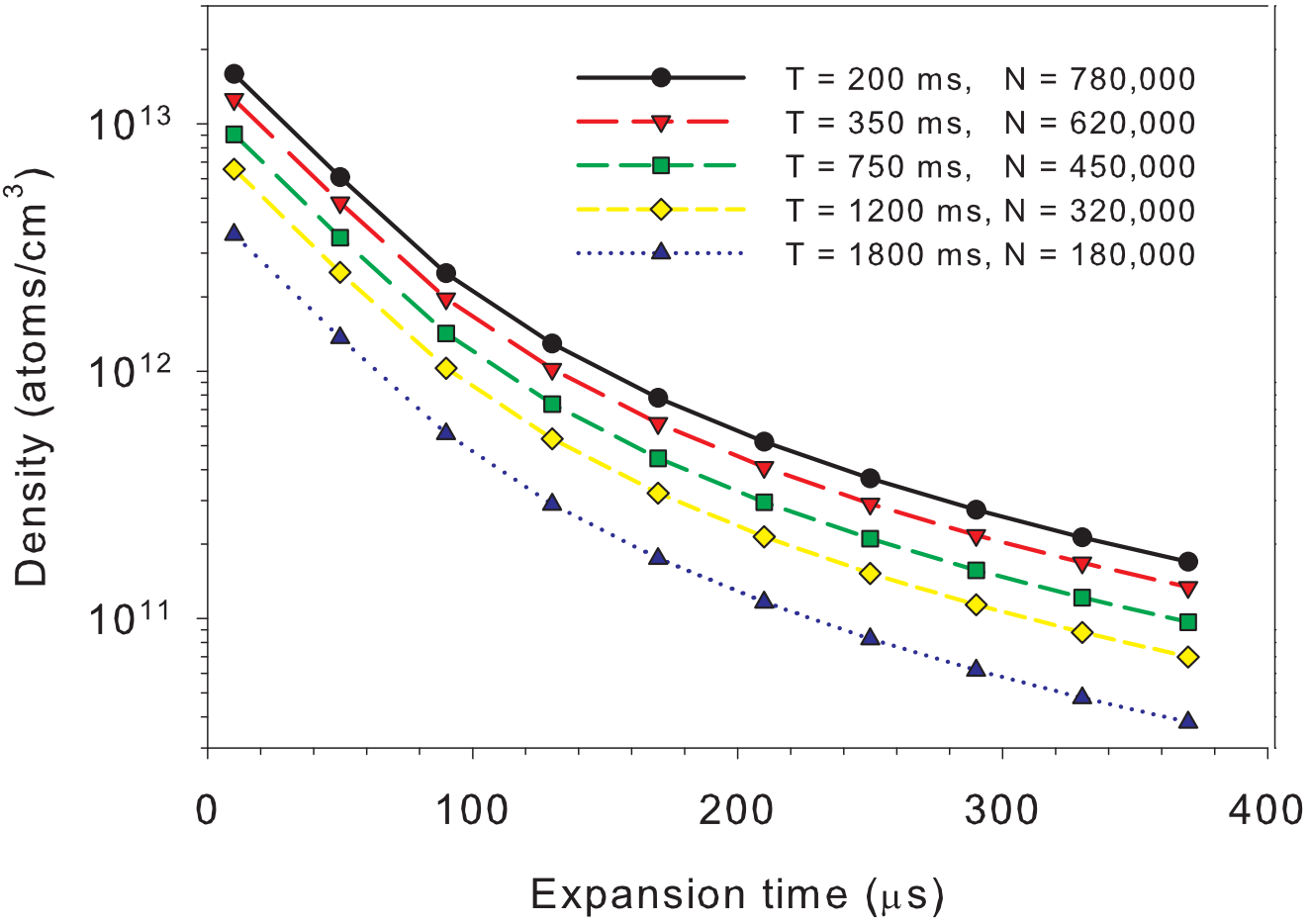

FIG. 2: Reduction of the number of atoms within the FORT over time due to ballistic expansion, thermalization and background gas collisions. After various hold times T there are N atoms in the trap (see legend). After the FORT trapping laser is extinguished, the sample expands, reducing the peak atomic density as shown.

III. RESULTS AND DISCUSSION

In this section we present our experimental results and make side by side comparison of the measurements and fully quantum calculations of the measured quantities. These results and comparisons are followed by two subsections in which the data is globally analyzed and discussed in terms of attenuation of the propagating light beam and a random walk for the diffusing light.

The details of the microscopic calculational techniques are described in detail in several earlier papers [2, 31, 32] on the general subject of light scattering in a cold and dense gas. For completeness, we include here a brief overview of this model. Our approach is one of the versions of the method known in the literature as the coupled dipoles (CD) model. This model has been heavily used in the context of cooperative scattering (see references in the introduction and see also [35–39]). In our variant of the CD approach we solve the nonstationary Schrodinger equation for the wave function ψ of the joint system consisting of N motionless two-level atoms (ground state with the total angular

momentum $J_g = 0$, and degenerate excited state $J_e = 1$ with $m = J_z = 1, 0, -1$) and a weak electromagnetic field. A vacuum reservoir is also included in our considerations. We search for the wave function ψ as an expansion in a set of eigenfunctions of the Hamiltonian of the noninteracting atoms and field. For the considered case of weak excitation (linear optics regime), we account only for states with no more than one photon in the field. Tracing over the photon degrees of freedom we obtain a finite set of equations for the Fourier component of amplitudes of states with one excited atom, which are the basic equations of the CD model. This set of equations is solved numerically.

The resulting solution gives us the opportunity to find all the other amplitudes of the states taken in our consideration and consequently the approximate wave function of the studied joint physical system. Knowledge of the wave function allows us to describe the properties of the atomic ensemble as well as the properties of the secondary radiation. Particularly, we can calculate the intensity of the different polarization components of the light scattered in an arbitrary direction as a corresponding quantum-mechanical average (for more detail see [32]. Possible atomic displacement caused by residual atomic motion is taken into account in our approach by averaging of calculated quantities over this random spatial distribution of the atoms. Theoretical results obtained in the framework of this procedure are scaled [33] to account for the fact that the measurements and theoretical calculations are made at very different numbers of atoms.

In this section we present our experimental results and make side by side comparison of the measurements and fully quantum calculations of the measured quantities. The details of the calculational techniques are described in detail in several earlier papers [2, 31, 32] on the general subject of light scattering in a cold and dense gas. Note that the theoretical results are scaled [33] to account for the fact that the measurements and theoretical comparisons are made at very different numbers of atoms. These results and comparisons are followed by two subsections in which the data is globally analyzed and discussed in terms of attenuation of the propagating light beam and a random walk for the diffusing light.

A. Experimental results and comparison with theory

We first point out that, in all cases, fluorescence measurements are made after the atoms in the FORT have essentially thermalized and the FORT has been turned off, so that the atoms are mainly in free space. There are two primary overlapping experimental protocols. In one, once the FORT has been extinguished, the expanding atomic sample is exposed to a series of ten $1\mu s$ probe pulses temporally spaced to map out a factor of several hundred in peak atomic density. As the probe spatial profile is much larger than the atomic sample, the number of atoms probed remains essentially constant. In a second protocol, the atom sample is held in the trap for increasingly longer periods of time; background gas collisions reduce the number of atoms in the ensemble, while the sample size, as measured by the sample Gaussian radii, remains the same. Then the FORT is extinguished and a sequence of probe pulses is used to probe the sample. This dual approach allows mapping out of both the atomic sample size and atomic density dependence of the fluorescence signals.

As an initial result, we present in Fig. 3 the measured fluorescence signals from a 10 μs probe pulse and their dependence on the peak atomic density. We see in the figure that the signals increase with decreasing atomic density. The origin of this somewhat counterintuitive effect arises from the fact that, for the highest densities, and consequently the greatest optical depth, the probe beam is attenuated during its traversal through the sample. The scattering signals

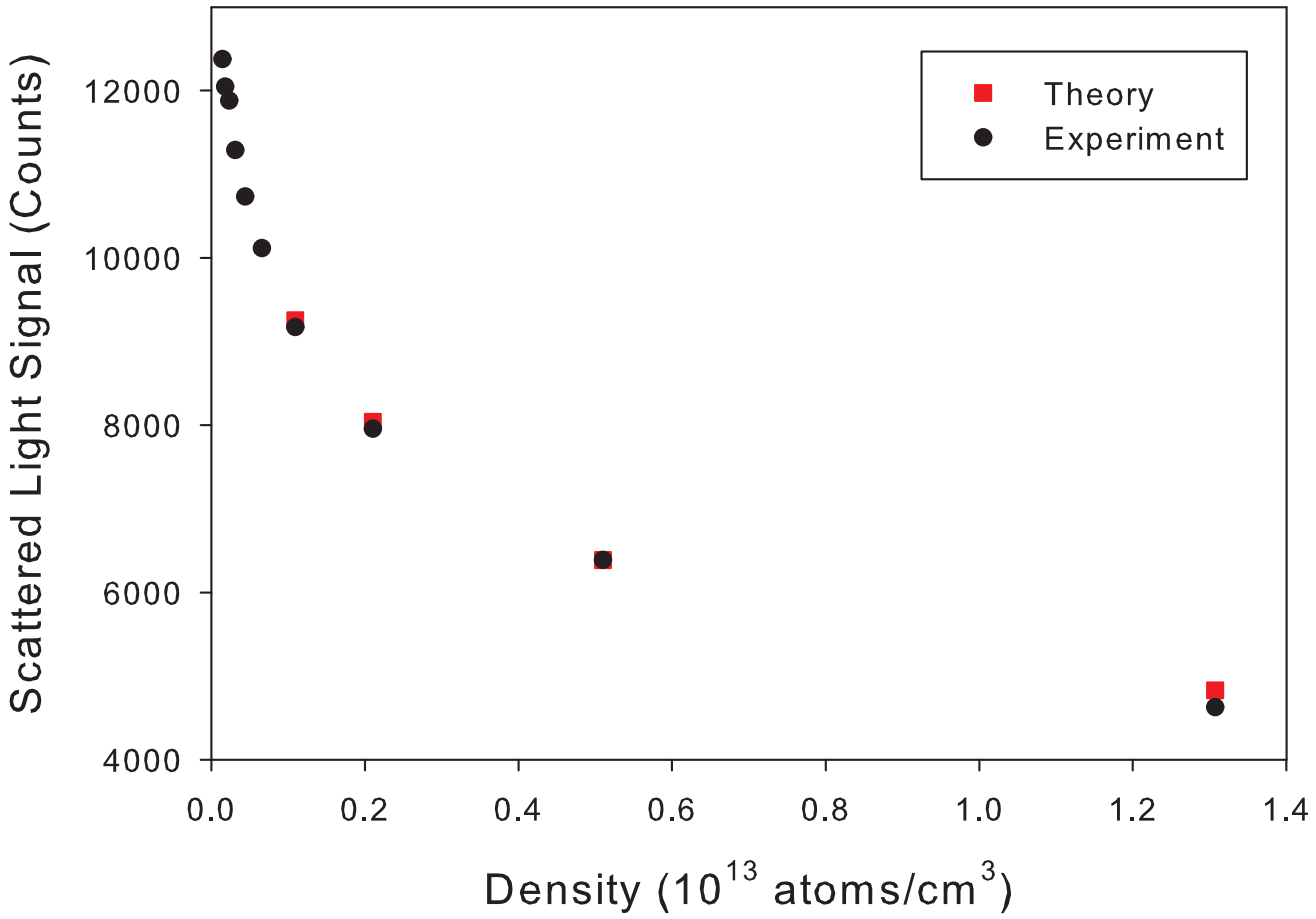

FIG. 3: On resonance variation of the scattered light signals with peak atomic density. Note the strong increase of the signal size with decreasing atomic density, for a fixed number of atoms in the sample.

then should originate mainly from light scattered from the illuminated outer regions of the sample surface, and the relatively fewer atoms compared to the sample as a whole. We will study in more detail this "shadow effect" in the next subsection. As the density is decreased, on the other hand, the sample becomes more optically thin; the sample ultimately scatters light as a collection of individual atoms. Comparison of the experimental results with calculations shows very good agreement. Note that the vertical (signal) scale is adjusted to match the experimental and theoretical responses.

We elaborated on this general effect by measuring the dependence of the scattering signals on atomic density and on detuning from atomic resonance. The overall experimental results for all positive blue detunings and densities are shown in Fig. 4(a). One striking feature of these results is that, for larger detunings, the sensitivity of the signals to decreases in the density is significantly reduced, and for the largest detunings from resonance, there is, within the experimental uncertainty, no variation of the signal intensity with peak atomic density. This effect is due to the decreasing optical depth of the atomic sample with increasing detuning; for the smallest optical depth, all the atoms experience essentially the same probe intensity, and thus contribute to the scattering signals. The corresponding theoretical results are shown Fig. 4(b). These results are in very good qualitative agreement with the experimental

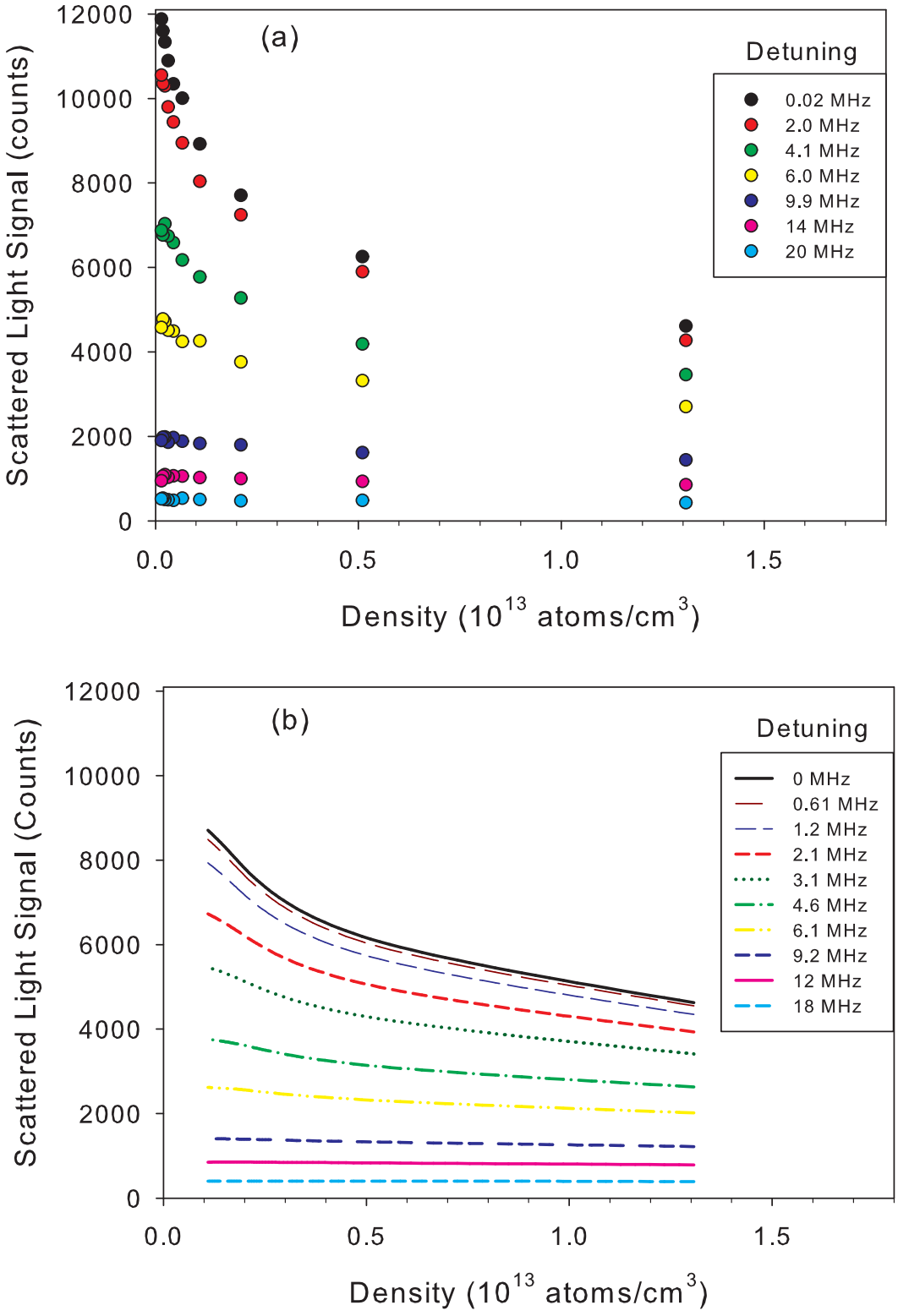

FIG. 4: Detuning and density dependence of the measured scattered light intensity. (a) Experimental results for positive (blue) detunings. (b) Theoretical results. The vertical scale has been adjusted to match the experimental data.

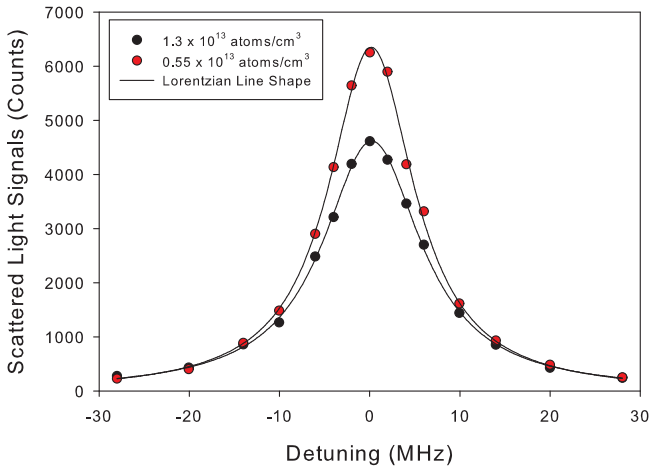

FIG. 5: Representative line shapes for the dependence of the measured signals on detuning from atomic resonance.

ones. Red detuned measurements (not shown) are also in very good agreement with the simulations. The data are also quite symmetric about zero detuning; this is seen in the characteristic spectral response for two different densities, as shown in Fig. 5. There the solid lines represent Lorentzian spectral profiles; this line shape is a very good empirical fit to the measured profile.

Implicit in Figs. 3 and Fig. 4 is a dependence on the spectral width (*viz*. Fig. 5) and the ensemble response to changes in atomic density. This dependence is shown in Fig. 6, where we see a nonlinear increase of the spectral width with increasing density, and an approach at low density to around 9 MHz, evidently larger than the 6.1 MHz expected for single scattering. This behavior should be compared to that reported by Pellegrino, *et al*, [27] in a recent paper. In our case, the lower density limit is partly due to the technical combination of the laser linewidth and the Doppler width of the transition. Further, this dependence is qualitatively due to the fact that major contributions to the signal arise from atoms near the outer regions of the atomic sample, the deeper atoms contributing less due to the shadow effect. For a large optical depth and a uniform density, this implies a roughly $\sqrt{b}$ scaling of the width; here b is the peak optical depth through the center of the sample [33]. A fit to the data in Fig. 6 leads to a low density intercept of around 7(1) MHz, in reasonable agreement with expectations. We should point out that, realistically, our samples are strongly inhomogeneous, and there are contributions to the signals from a range of atomic densities. Such scaling should then be considered as only a qualitative feature of the measured spectral widths.

Finally, we have examined the dependence of the measured scattered light intensity with variations in the effective volume of the sample. We use as a measure of the sample volume the product of the atom sample Gaussian radii, *viz*., $(2\pi)^{3/2} y_o r_o^2$. In these measurements, this product is held fixed as the number of atoms in the sample is varied. Results are shown in Fig. 7. We see in Fig. 7 that, for each sample size, and within the experimental uncertainty, the signal increases monotonically with increasing number of atoms (or atomic density). However, the rate of increase is significantly different, depending on the sample size, and is strongly suppressed for the smallest sample sizes.

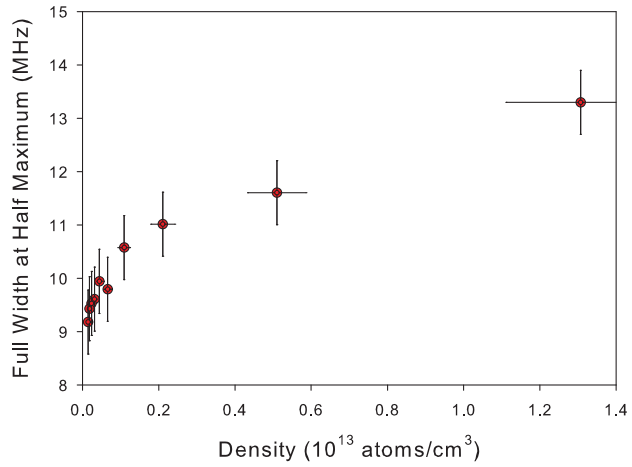

FIG. 6: Dependence of the full width at half maximum of the atomic resonance response as a function of atomic density. These measurements correspond to varying the density by changing the sample size while holding the number of atoms fixed.

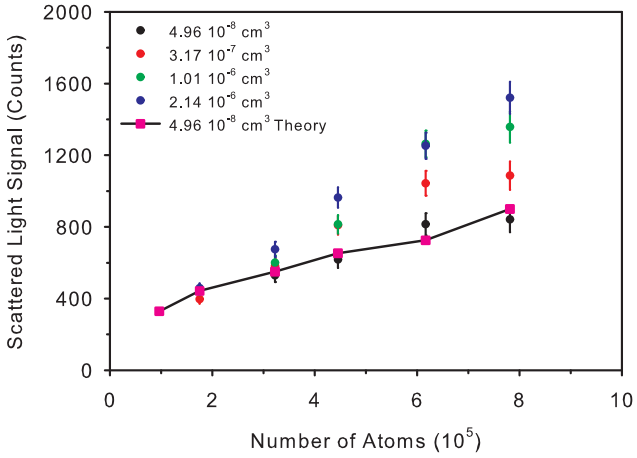

FIG. 7: Representative atom number dependence of the scattering signals as a function of the cold atom sample size. The data is labeled according to the volume of the sample, as described in the text.

B. Rescaling according to the Beer-Lambert Law

The good agreement between the data and the full microscopic theory is in itself satisfactory but it does not allow identifying the relevant physical ingredients at the origin of the specific behavior of the scattered light as a function of the different control parameters. This is because the microscopic theory naturally contains many effects: attenuation of the probe light, diffraction and refraction, multiple scattering, super and subradiance, collective shifts, etc. It is thus useful to compare the data with a much simplified theory, including only some of these effects.

An effective approximation could be based on the ladder-type expansion of the light correlation function, which leads to a Bethe-Salpeter type equation. This can be numerically solved via a sequence of iterative steps (multiple scattering events), see [2]. Such an approach evidently ignores any cross interference in the process of multiple scattering, which seems a rather realistic assumption for a dilute and disordered atomic gas. The applicability of the

Bethe-Salpeter approach has been successfully demonstrated for the theory of random lasing, see [34, 40]

In this section, we show that taking into account only attenuation of the probe beam in the atomic sample, following the Beer-Lamabert Law, is enough to explain the data with rather good agreement. This shows that the main physical ingredient of the experiment is the so-called "shadow effect": atoms at the back of the sample are less illuminated by the incident laser, which induces an effective reduction of the total scattering cross-section compared to a collection of independent atoms illuminated by the same laser intensity. As explained in detail in [41], this effect also explains previous observations of a collective reduction of the radiation pressure force [6, 8]. It could also explain the results of [27], although the very small sample sizes and high densities used in that work might induce some other effects.

From the Beer-Lambert Law, one can easily show (see Appendix A or ref. [8]) that the total scattering cross-section of a Gaussian cloud (containing N atoms and illuminated by a plane wave) is

$$\Sigma_{\rm sc} = N\sigma_{\rm sc} \times \frac{\mathrm{Ein}(b)}{b}\,, \tag{1}$$

where Ein is the integer function [42]

$$\begin{aligned}\mathrm{Ein}(b) &= \int_0^b \frac{1-e^{-x}}{x}\,dx \\ &= b\left[1+\sum_{n=1}^{\infty}\frac{(-b)^n}{(n+1)(n+1)!}\right],\end{aligned} \tag{2}$$

and $\sigma_{\rm sc}$ is the single-atom scattering cross-section. Here b is the optical depth along the line of sight and the factor $\mathrm{Ein}(b)/b$ in Eq. 1 corresponds to the deviation from single-atom physics induced by the shadow effect. In the limit of vanishing optical depth b, the value expected from single atom physics is recovered, $\Sigma_{\rm sc} = N\sigma_{\rm sc}$. For high optical depth, the cross-section increases only logarithmically, which appears as a collective saturation of the scattered light.

Let us now use this result to rescale the experimental data. The measured scattered light is proportional to $\Sigma_{\rm sc}$. For data taken with a fixed atom number and varying detuning ("protocol 1"), such as the data reported in Fig. 4(a) and Fig. 5, one should divide the signal by $\sigma_{\rm sc} \propto 1/(1+4\Delta^2/\Gamma^2)$ and compare the results to $\mathrm{Ein}(b)/b$. For data acquired at a fixed detuning and varying atom number ("protocol 2"), such as the data reported in Fig. 7, one should divide the signal by N and also compare to $\mathrm{Ein}(b)/b$. In both cases one has to allow a global multiplicative factor to fit the data to the theoretical curve, since the signal is not calibrated in absolute value. In other words, the detection efficiency, which is the number of detected photons *vs.* the number emitted in the detector direction, is not precisely known. The not-very-well known factors include the detector solid angle, the absolute probe intensity and the probe overlap with the sample spatial location, the transmission of the various optical elements in the detector arm of the apparatus, and the efficiency of the light detector to incoming photons. The relevant optical depth b is the one along the line of sight of the laser, given by

$$b = \frac{\sqrt{2\pi}\rho_0\sigma_{\rm sc}r_0}{\sqrt{\cos^2\theta + \sin^2\theta\sin^2\phi + \eta^2\sin^2\theta\cos^2\phi}}\,, \tag{3}$$

where $\eta = r_0/y_0$, r_0, y_0, ρ_0 vary during the expansion and the angles θ, ϕ are given by the geometry of the experiment as shown in Fig. 1 ($\theta = 23°$ and $\phi = 30°$).

We show the rescaled data in Fig. 8. The two panels correspond to the two different experimental protocols. The striking result is that, despite the different protocols and different orders of magnitudes (almost 3 orders of magnitude in density and in optical depth), all data points collapse quite close to the curve $\mathrm{Ein}(b)/b$ describing the shadow effect, demonstrating that it is indeed the main physical ingredient of the collective behavior of the scattered light intensity.

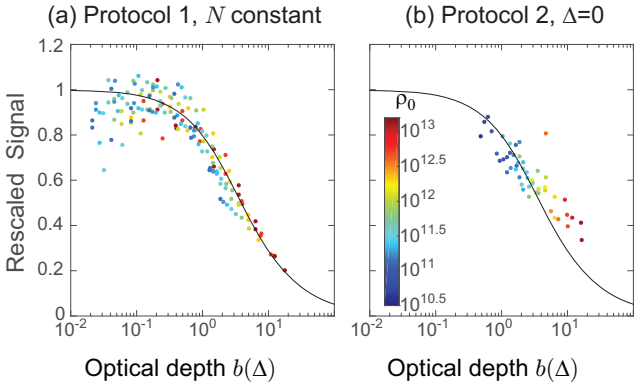

FIG. 8: Rescaled experimental data: the light scattering signal is plotted as a function of the detuning-depended optical depth $b(\Delta)$ and the color code indicates the peak density ρ_0 in cm^{-3} (log scale). The solid line is the function $\mathrm{Ein}(b)/b$ which describes the shadow effect from the Beer-Lambert Law. The two panels correspond to the two different experimental protocols, the first one with a varying detuning and a constant atom number, the second one with the laser on resonance and a varying atom number. In both cases the sizes of the cloud also vary, and thus the volume and density. A global vertical scaling factor for each data set is the only free parameter.

C. Impact of multiple scattering

The previous scaling based on the total scattering cross-section supposes that the light is emitted isotropically from the atomic sample. This is not the case when the optical depth is large, as already studied in [4], although the anisotropy is much less pronounced when the cloud is illuminated by a wide beam (plane wave), as is the case here, compared to the case when a large cloud is illuminated by a narrow beam, as in [4].

To describe this effect one needs to take into account multiple scattering of light inside the sample. This is naturally included in the microscopic model, but it is also possible to use stochastic simulations based on a random walk algorithm for light. In such a model, cooperative and coherent effects such as super and subradiance, interference and diffraction are neglected, but one can well describe diffuse light scattering with the true parameters of the experiments (also including subtle effects like the frequency redistribution due to Doppler broadening), if needed, see e.g. [43–45].

We have performed such random walk simulations for varying optical depths. The simulations include the actual geometry of the laser beam (size and direction) and of the detection (direction), the anisotropy of the scattering diagram for the first scattering event and the Gaussian density distribution of the cloud. We use the size y_0 of the cloud, which is almost constant for all data points, and the two extreme transverse sizes, corresponding to the shortest and longest time of flight. We do not take into account the Doppler-induced frequency redistribution during multiple scattering as it should be a tiny effect with the moderate temperature and optical depths explored here. The results are shown in Fig. 9.

The comparison between the random walk simulations and the simple Beer-Lambert prediction shows a small difference: the scattered light signal is always slightly larger in the random walk simulations. Several contributions explain this difference. First, the Gaussian beam profile has a stronger intensity at the center, where it interacts with the cloud, compared with a plane-wave illumination. Second, the small anisotropy of the scattering diagram of Rb (we suppose an equally populated mixture of Zeeman states) slightly favors the direction of detection. And third, at

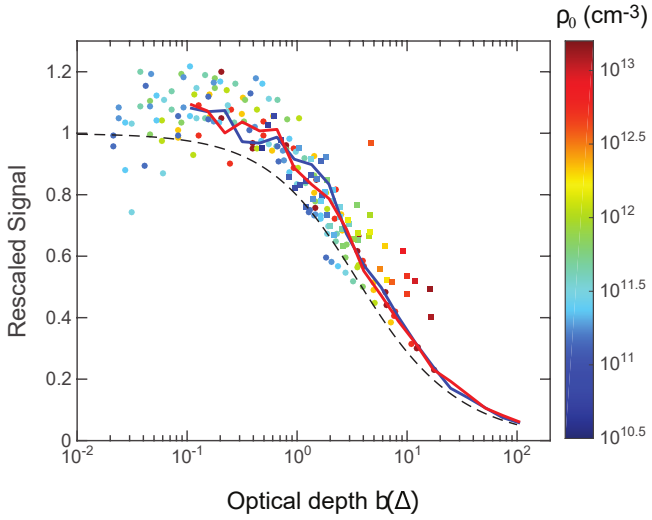

FIG. 9: Comparison between the experimental data and the random walk simulation. The data are rescaled like in Fig. 8, dots corresponds to the protocol 1 and squares to the protocol 2. The color code indicates the peak density ρ_0 in cm^{-3} (log scale). The solid lines are the results of the random walk simulations for the two extreme aspect ratios of the cloud, $\eta = r_0/y_0 \simeq 0.13$ (blue) and $\eta \simeq 0.013$ (red). The dashed line is the function $\mathrm{Ein}(b)/b$ which describes the shadow effect from the Beer-Lambert Law. The global vertical scaling factor for each data set has been adapted to match the random walk results.

large optical depths, multiple scattering takes place and light has a higher probability to escape along the backward and transverse directions, which also favors the detection direction compared to an isotropic emission. Finally, at the precision of the numerical simulation, we do not see any significant difference between the two extreme aspect ratios of the cloud, showing that this parameter does not affect the results. In Fig. 9, the vertical scaling factor of each data set has been chosen to match the simulation results. With this as the only free parameter the simulations and the experimental points are in very good agreement.

IV. CONCLUSIONS

Using two different experimental protocols, we have made measurements of diffusive light scattering from a cold thermal gas of ^{87}Rb. Due to variations in the number of atoms in the sample, or the size of the sample at fixed number of atoms, the experiments extended over almost 3 orders of magnitude in density and in optical depth. The measured diffusive light spectra were found to be in very good agreement with fully quantum based calculations. A second and simpler analysis approach used stochastic simulations based on a random walk algorithm for the multiply scattered light. The simulations revealed that the optical depth of the atomic sample can serve as an effective single scaling parameter which describes very well all the experimental data. A final but important overall point, as mentioned earlier in the paper, is that a substantial portion of the scattered light undergoes multiple scattering. However, the multiple scattering only contributes a little to the emission diagram. With this, and the global scale factor needed to compare the data and Beer-Lambert Law scaling, we can emphasize that the Beer-Lambert Law works in spite of multiple scattering. This concluding point demonstrates the effectiveness of this rescaling.

Acknowledgments

We appreciate financial support by the National Science Foundation (Grant No. NSF-PHY-1606743 and NSF-PHY-1939308), the Russian Foundation for Basic Research (Grant No. 18-02-00265), the Russian Scientific Foundation (Grant No. 18-72-10039), and the French Agence Nationale pour la Recherche (project LOVE, No. ANR-14-CE26-0032). The quantum microscopic calculations were financially supported by the Russian Science Foundation under Project 17-12-01085.

Appendix A: Proof of Eq. (1) for the shadow effect

For simplicity, let us take an isotropic Gaussian cloud with density distribution $\rho = \rho_0 e^{-r^2/(2R^2)}$ and consider a plane wave (intensity I_0) propagating along z. The transmitted intensity has a transverse distribution

$$\begin{aligned} I_T(\mathbf{r}_\perp) &= I_0 \exp\left(-\rho_0 \sigma_{\rm sc} \int e^{-r^2/(2R^2)} dz\right) \\ &= I_0 \exp\left(-b e^{-r_\perp^2/(2R^2)}\right) , \end{aligned} \tag{A1}$$

with $b = \sqrt{2\pi}\rho_0 \sigma_{\rm sc} R$ and $\mathbf{r}_\perp = (x, y)$.

Moreover, what is scattered is what is not transmitted, so we have

$$\Sigma_{\rm sc} = \frac{P_{\rm sc}}{I_0} = \int \left[1 - \exp\left(-b e^{-r_\perp^2/(2R^2)}\right)\right] d^2\mathbf{r}_\perp \, . \tag{A2}$$

Using $d^2\mathbf{r}_\perp = 2\pi r_\perp dr_\perp$ and the change of variable $u = b e^{-r_\perp^2/(2R^2)}$ one obtains

$$\Sigma_{\rm sc} = 2\pi R^2 \int_0^b \frac{1 - e^{-u}}{u} du = 2\pi R^2 {\rm Ein}(b). \tag{A3}$$

For single atom physics, the total cross section would be $N\sigma_{\rm sc}$. Using $b = \sigma_{\rm sc}/(2\pi) \times N/R^2$, it is thus physically meaningful to write

$$\Sigma_{\rm sc} = N\sigma_{\rm sc} \times \frac{{\rm Ein}(b)}{b} \, , \tag{A4}$$

which is Eq. (1).

[1] W. Guerin, M. T. Rouabah, and R. Kaiser, J. Mod. Opt. **64**, 895 (2017).

[2] D. V. Kupriyanov, I. M. Sokolov, and M. D. Havey, Phys. Rep. **671**, 1 (2017).

[3] S. Roof, K. Kemp, M. D. Havey, I. M. Sokolov, and D. V. Kupriyanov, Opt. Lett. **40**, 1137 (2015).

[4] G. Labeyrie, D. Delande, C. A. Müller, C. Miniatura, and R. Kaiser, Opt. Commun. **243**, 157 (2004).

[5] R. Saint-Jalm, M. Aidelsburger, J. L. Ville, L. Corman, Z. Hadzibabic, D. Delande, S. Nascimbène, N. Cherroret, J. Dalibard, and J. Beugnon, Phys. Rev. A **in press** (2018), arXiv:1802.04018.

[6] T. Bienaimé, S. Bux, E. Lucioni, P. W. Courteille, N. Piovella, and R. Kaiser, Phys. Rev. Lett. **104**, 183602 (2010).

[7] H. Bender, C. Stehle, S. Slama, R. Kaiser, N. Piovella, C. Zimmermann, and P. W. Courteille, Phys. Rev. A **82**, 011404(R) (2010).

[8] J. Chabé, M. T. Rouabah, L. Bellando, T. Bienaimé, N. Piovella, R. Bachelard, and R. Kaiser, Phys. Rev. A **89**, 043833 (2014).

[9] D. E. Chang, J. Ye, and M. D. Lukin, Phys. Rev. A **69**, 023810 (2004).

[10] R. Friedberg, S. R. Hartmann, and J. T. Manassah, Phys. Rep. **7**, 101 (1973).

[11] M. O. Scully, Phys. Rev. Lett. **102**, 143601 (2009).

[12] M. O. Scully and A. A. Svidzinsky, Science **328**, 1239 (2010).

[13] J. T. Manassah, Adv. Opt. Photon. **4**, 108 (2012).

[14] J. Javanainen, J. Ruostekoski, Y. Li, and S.-M. Yoo, Phys. Rev. Lett. **112**, 113603 (2014).

[15] J. Javanainen and J. Ruostekoski, Opt. Express **24**, 993 (2016).

[16] R. Röhlsberger, K. Schlage, B. Sahoo, S. Couet, and R. Rüffer, Science **328**, 1248 (2010).

[17] J. Keaveney, A. Sargsyan, U. Krohn, I. G. Hughes, D. Sarkisyan, and C. S. Adams, Phys. Rev. Lett. **108**, 173601 (2012).

[18] S. Okaba, T. Takano, F. Benabid, T. Bradley, L. Vincetti, Z. Maizelis, V. Yampol'skii, F. Nori, and H. Katori, Nat. Commun. **5**, 4096 (2014).

[19] Z. Meir, O. Schwartz, E. Shahmoon, D. Oron, and R. Ozeri, Phys. Rev. Lett. **113**, 193002 (2014).

[20] S. L. Bromley, B. Zhu, M. Bishof, X. Zhang, T. Bothwell, J. Schachenmayer, T. L. Nicholson, R. Kaiser, S. F. Yelin, M. D. Lukin, et al., Nat. Commun. **7**, 11039 (2016).

[21] S. Jennewein, M. Besbes, N. J. Schilder, S. D. Jenkins, C. Sauvan, J. Ruostekoski, J.-J. Greffet, Y. R. P. Sortais, and A. Browaeys, Phys. Rev. Lett. **116**, 233601 (2016).

[22] S. J. Roof, K. J. Kemp, M. D. Havey, and I. M. Sokolov, Phys. Rev. Lett. **117**, 073003 (2016).

[23] L. Corman, J. L. Ville, R. Saint-Jalm, M. Aidelsburger, T. Bienaimé, S. Nascimbène, J. Dalibard, and J. Beugnon, Phys. Rev. A **96**, 053629 (2017).

[24] S. Jennewein, L. Brossard, Y. R. P. Sortais, A. Browaeys, P. Cheinet, J. Robert, and P. Pillet, Phys. Rev. Lett. **116**, 233601 (2016).

[25] S. Balik, A. L. Win, M. D. Havey, I. M. Sokolov, and D. V. Kupriyanov, Phys. Rev. A **87**, 053817 (2013).

[26] S. Balik, A. L. Win, M. D. Havey, A. S. Sheremet, I. M. Sokolov, and D. V. Kupriyanov, J. Mod. Opt. **61**, 77 (2014).

[27] J. Pellegrino, R. Bourgain, S. Jennewein, Y. R. P. Sortais, A. Browaeys, S. D. Jenkins, and J. Ruostekoski, Phys. Rev. Lett. **113**, 133602 (2014).

[28] R. G. Olave, A. L. Win, K. Kemp, S. J. Roof, S. Balik, M. D. Havey, I. M. Sokolov, and D. V. Kupriyanov, *From atomic to mesoscale: The role of quantum coherence in systems of various complexities* (World Scientific, 2015), chap. Optical manipulation of light scattering in cold atomic rubidium, arXiv:1406.5783.

[29] Y.-C. Chen, Y.-A. Liao, and I. A. Yu, Phys. Rev. A **64**, 031401(R) (2001).

[30] S. Balik, R. Olave, C. I. Sukenik, M. D. Havey, V. M. Datsyuk, I. M. Sokolov, and D. V. Kupriyanov, Phys. Rev. A **72**, 051402(R) (2005), URL `https://link.aps.org/doi/10.1103/PhysRevA.72.051402`.

[31] I. M. Sokolov, M. D. Kupriyanova, D. V. Kupriyanov, and M. D. Havey, Phys. Rev. A **79**, 053405 (2009).

[32] I. Sokolov, D. Kupriyanov, and M. Havey, JETP **112**, 246 (2011).

[33] I. M. Sokolov, A. S. Kuraptsev, D. V. Kupriyanov, M. D. Havey, and S. Balik, J. Mod. Opt. **60**, 50 (2013).

[34] L. V. Gerasimov, V. M. Ezhova, D. V. Kupriyanov, Q. Baudouin, W. Guerin, and R. Kaiser, Phys. Rev. A **90**, 013814 (2014).

[35] J. Ruostekoski and J. Javanainen, Phys. Rev. A 55, 513 (1997).

[36] A. A. Svidzinsky, J. Chang, and M. O. Scully, Phys. Rev. A 81, 053821 (2010).

[37] A. S. Kuraptsev, I. M. Sokolov and M. D. Havey, Phys. Rev. A 96 023830 (2017).

[38] D. V. Kuznetsov, V. K. Roerich, and M. G. Gladush, JETP. 113, 647 (2011).

[39] T. Bienaim, R. Bachelard, P. W. Courteille, N. Piovella, and R. Kaiser, Fortschr. Phys. 61, 377 (2013).

[40] L. Gerasimov, D. Kupriyanov, and M. Havey, Optics and Spectroscopy **119**, 403 (2015).

[41] R. Bachelard, N. Piovella, W. Guerin, and R. Kaiser, Phys. Rev. A **94**, 033836 (2016).

[42] E. W. Weisstein, *Ein function*, From MathWorld–A Wolfram Web Resource. http://mathworld.wolfram.com/EinFunction.html.

[43] G. Labeyrie, E. Vaujour, C. A. Müller, D. Delande, C. Miniatura, D. Wilkowski, and R. Kaiser, Phys. Rev. Lett. **91**, 223904 (2003).

[44] A. Eloy, Z. Yao, R. Bachelard, W. Guerin, M. Fouché, and R. Kaiser, Phys. Rev. A **97**, 013810 (2018).

[45] P. Weiss, M. O. Araújo, R. Kaiser, and W. Guerin, New. J. Phys. **20**, 063024 (2018), URL `https://doi.org/10.1088/1367-2630/aac5d0`.